



Stratigraphic Characteristics and Sediment-Filling Process of the Early Permian Fengcheng Formation in the Northwestern Margin of the Junggar Basin, Northwest China

Dongming Zhi^{1,2}, Mingxin Liu³, Xinwei Chen³, Nuru Said^{4,5}, Wenbin Tang³, Chenhui Hu³, Zhijun Qin¹, Hao Zou^{3*} and Deyu Gong^{6*}

¹Xinjiang Oilfield Company, PetroChina, Karamay, China, ²Turpan-Hami Oilfield Company, PetroChina, Hami, China, ³State Key Laboratory of Oil and Gas Reservoir Geology and Exploitation, Chengdu University of Technology, Chengdu, China, ⁴Department of Mineral and Rocks, King Abdul-Aziz University, Jeddah, Saudi Arabia, ⁵Centre of Exploration Targeting, The University of Western Australia, Crawley, WA, Australia, ⁶Research Institute of Petroleum Exploration and Development, PetroChina, Beijing, China

OPEN ACCESS

Edited by:

Shang Xu,
China University of Petroleum, China

Reviewed by:

Zeyang Liu,
Guangzhou Institute of Geochemistry
(CAS), China
Kuanhong Yu,
China University of Petroleum, China

*Correspondence:

Hao Zou
zouhao@cduet.edu.cn
Deyu Gong
deyugong@126.com

Specialty section:

This article was submitted to
Economic Geology,
a section of the journal
Frontiers in Earth Science

Received: 16 May 2022

Accepted: 14 June 2022

Published: 08 August 2022

Citation:

Zhi D, Liu M, Chen X, Said N, Tang W,
Hu C, Qin Z, Zou H and Gong D (2022)
Stratigraphic Characteristics and
Sediment-Filling Process of the Early
Permian Fengcheng Formation in the
Northwestern Margin of the Junggar
Basin, Northwest China.
Front. Earth Sci. 10:945563.
doi: 10.3389/feart.2022.945563

The Permian Fengcheng Formation in the Mahu sag of the Junggar Basin is a crude oil reservoir and source rock. However, its stratigraphic characteristics, the boundary marks of the three members (lower, middle, and upper), and the sediment-filling processes are unclear. This study presents the sedimentary systems and sediment-filling processes in an intracontinental rift basin of this area using sedimentary-faces analysis, sequence stratigraphy, well logs, and two-dimensional seismic interpretations. The results show that the Fengcheng Formation consists of three third-order sequence stratigraphy (SQf1, SQf2, and SQf3). The lowest member of the Fengcheng Formation is composed of gray to dark gray thin middle layers of tuff, lacustrine dolomitic mudstone, and argillaceous dolomite near the depocenter. Tuff, siltstone, a small amount of fan-delta glutenite, volcanic breccia, and basalt are present near the fault zone. The logging curve is characterized by a high gamma-ray (GR) value, high amplitude, wavelength growth, and medium frequency. Near the depocenter, the middle member of the Fengcheng Formation comprises gray and gray-black thin layers of lacustrine muddy dolomite and dolomitic mudstone and thin sandstone and mudstone interbedded between tuff and gravel near the orogenic belt. The logging curve displays high-to-low GR values, high amplitude, short wavelength, and high frequency. The upper member of the Fengcheng Formation is not characterized by lesser tuffaceous and dolomitic components but by an increased fan-delta sandy content. Next, the bottom of the upper member is composed of lacustrine mudstone and siltstone interbedded between dolomitic mudstones; whereas, the top of the upper member is dominated by fan-delta coarse sandstone and sandy conglomerate. The logging curve shows low GR values, small amplitude, and continuous stability. The sediment-filling process of the Fengcheng Formation is controlled by fault activity. Overall, the lower and middle members of the Fengcheng Formation expand during the sediment-filling process of the lake basin of the Mahu sag; whereas, the upper member contracts. The strong uplift of the Horst near the Baiquan and Mahu orogenic

belts led to an increase in provenance supply, resulting in a contraction of the southwestern margin of the lake basin during the sedimentation period from lower member to upper member of Fengcheng Formation.

Keywords: stratigraphic characteristics, sediment-filling process, Mahu sag, early Permian Fengcheng Formation, Junggar Basin

1 INTRODUCTION

Junggar Basin is a large petroliferous superimposed basin in northwest China (Cao et al., 2006; Jia et al., 2010; Zhang et al., 2010; Zhang et al., 2015; Li, 2022). The Permian delta sandstone, shore–shallow lacustrine, and semideep lacustrine mudstone developed in the Junggar Basin are the most critical reservoirs and source rocks, respectively (Gong et al., 2018; Gong et al., 2020). The volume of Permian oil and gas resources ranks first among all strata in the Junggar Basin. The Mahu sag, in the northwestern margin of the Junggar Basin, is a hydrocarbon-rich sag with the highest organic-matter content (Lei et al., 2014; Fang et al., 2019). The alkaline lacustrine sediments of the early Permian Fengcheng Formation in the Mahu sag are important source rocks for forming Karamay–Wuerhe and Mahu oil fields at the northwestern margin of the basin (Lei et al., 2005; Kuang and Qi, 2006; Zhang, 2013; Ouyang et al., 2018; Li et al., 2020; Tang et al., 2020). A detailed study of oil and gas exploration indicates that the Fengcheng Formation is a high-quality source rock and reservoir, forming conventional structural lithologic and unconventional tight/shale oil reservoirs (Wei et al., 2018; Zhi et al., 2019). Zhi et al. (2021) presented the orderly coexistence and accumulation models for conventional and unconventional hydrocarbons in the Lower Permian Fengcheng Formation. The Fengcheng Formation is divided into three members based on different lithologic assemblages (Cao et al., 2015), the characteristics of the sedimentary environment, and the development of the reservoir, tectonics, volcanism, and genesis of the rock, which are well documented (Xian, 1985; Niu et al., 2009; Liu et al., 2013; Gong et al., 2014). Chen et al. (2010) attempted to establish the sequence-division scheme of the Permian in the Wuxia area, in the northwest margin of the Junggar Basin, using a comprehensive analysis of well-seismic and -framework sequence. However, stratigraphic sequences and sediment-filling processes of the Fengcheng Formation are poorly understood.

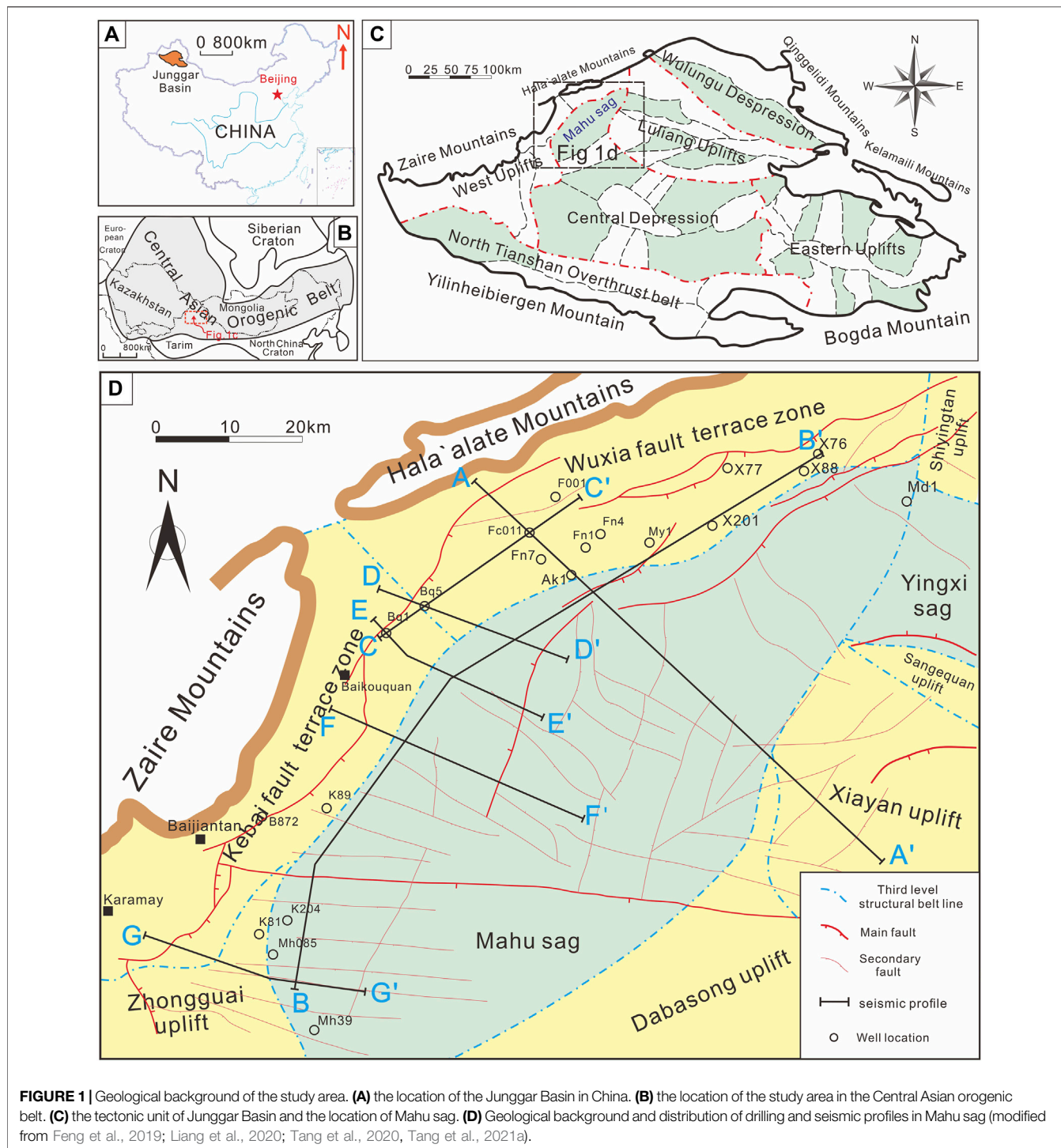
The division of these three members is important for accurate stratigraphic correlation and refined exploration. This study presents a detailed stratigraphic framework for the Fengcheng Formation based on core observation, logging curve, and seismic data. The objective of this study is to determine the stratigraphic characteristics and sedimentary-filling process of the early Permian Fengcheng Formation.

2 GEOLOGICAL SETTING

The Junggar Basin, located in northern Xinjiang, China (Figure 1A) (He et al., 2004a), is an important part of the

Central Asian Orogenic Belt (Shi et al., 2017; Pei et al., 2018; Zhang et al., 2020). It is located at the junction of Kazakhstan, Siberian, and Tarim Blocks (Figure 1B) (He et al., 2018). The basin is a late Paleozoic, Mesozoic, and Cenozoic superimposed basin (Cao et al., 2006; Zhang et al., 2010; Jin., 2011; Lu et al., 2019). The triangular Junggar Basin demonstrates an east–west extension, a width, and an area of ca. 700, 370, and 1.3×10^5 km², respectively. It is surrounded by the Zaire and Hala'alate mountains to the northwest; the Altai, Qingggelidi, and Kelamaili mountains to the northeast; and the Yilin Block, Biergen, and Bogda mountains to the south (Figure 1C). The Mahu sag is a second-order structural unit in the Junggar Basin, located at the northwest margin of the Junggar Basin (Figure 1C). The Mahu sag is a gentle-slope structure with monocline tilting to the southeast. Kebai (Karamay–Baikouquan) and Wuxia (Wuerhe–Xiazijie) fault zones are the main factors controlling the distribution and variation of the Permian–Triassic stratigraphic units (He et al., 2004b; Yu et al., 2016; Liang et al., 2020). The southeast slope belt of the sag is adjacent to the Shiyintan uplift, Yingxi sag, Sanquan uplift, Xiayan uplift, and Dabasong uplift, from north to south (Gong et al., 2019) (Figure 1D).

Since the late Carboniferous, after the southwestern part of the Central Asian orogenic belt was amalgamated, the Junggar Basin experienced multistage intraplate tectonic deformation (Hendrix et al., 1992; Carroll et al., 1995; Han et al., 2010; Wang et al., 2018). Thus, the Mahu sag has changed from an early Permian syn-rift basin to a middle Permian postrift basin, and the sedimentary range has expanded, ending with the tectonic inversion, from the late Permian to early Triassic (Tang et al., 2020, 2021a, b, c). The basement of the Mahu sag is a late Carboniferous arc-basin system (Li et al., 2016; Tang et al., 2020). The Carboniferous strata are sequentially overlain by the Permian Jiamuhe (P_1j), Fengcheng (P_1f), Xiazijie (P_2x), lower Wuerhe (P_2w), upper Wuerhe (P_3w), Triassic Baikouquan (T_1b), Karamay (T_2k), and Baijiantan (T_3b) Formations (Figure 2). The maximum thickness of the sedimentary center of the Mahu sag is more than 6,000 m. The Lower Permian Fengcheng Formation is the sedimentary response to the syn-rift II stage (Tang et al., 2021a). From the bottom to the top, the Fengcheng Formation of the Lower Permian can be divided into three members: the lower (P_1f^1), middle (P_1f^2), and upper members (P_1f^3). The P_1f^2 is dominated by mafic-intermediate volcanic rocks, coarse clastic rocks, organic-rich mudstones interbedded with dolomitic mudstones, tuffs, ignimbritic flows, and uniform organic-rich mudstone interval with interbedded tuff (He et al., 2018). The P_1f^2 is characterized by organic-rich mudstones and dolomitic mudstones with turbidite sandstones (Zhang et al., 2018). Next, the P_1f^3 contains mudstones with interbedded dolomitic mudstones in the lower part and terrigenous clastic rocks in the upper part (Cao et al., 2015).



3 MATERIALS AND METHODS

Investigation of the sedimentary characteristics, sequence stratigraphy, and filling process of the Fengcheng Formation is based on the analysis of two-dimensional (2D) seismic data, well logging, and core descriptions obtained from the Xinjiang Oil Company, PetroChina (**Figure 1D** for the location). Moreover, the seismic lines that were studied covered most of the western

margin of the Mahu sag. The 2D seismic profiles (SE-trending 110 km and NE-trending 290 km) demonstrated a record length of 7,500-m two-way travel. Therefore, penetration and resolution in all profiles are sufficient to image the Fengcheng Formation, representing our target. In addition, in this study, data from ten boreholes were combined and applied.

Sequence-boundary identification is the first step in the study of sequence stratigraphy (Vail, 1988). The base level is an

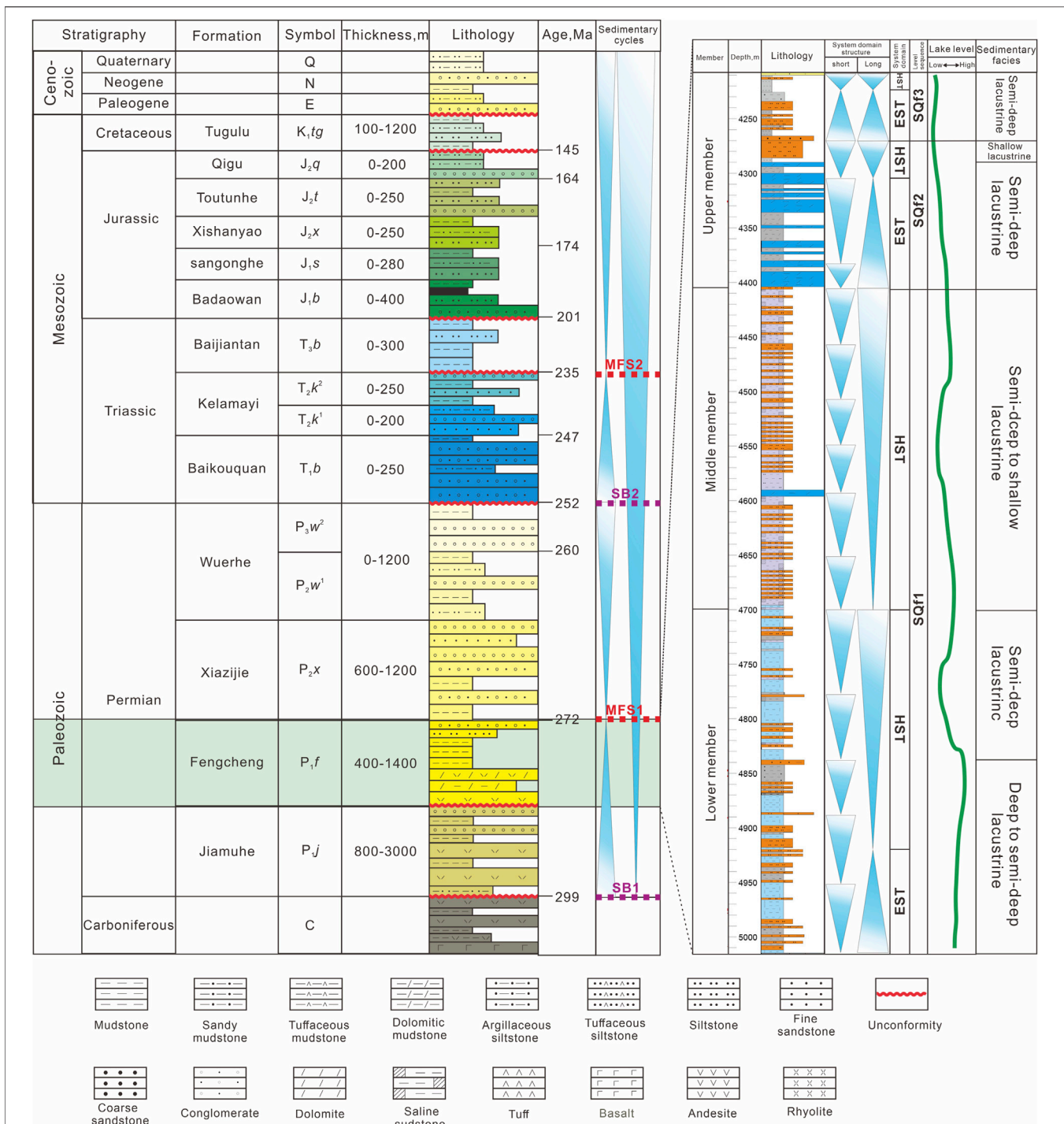


FIGURE 2 | Stratigraphic framework of the Paleozoic to Cenozoic in the Mahu sag (right) and lithologic column, sequence, and sedimentary facies of Fengcheng Formation in Fn7 well (left); SB, sequence boundary; MFS, maximum flooding surface (modified from Cao et al., 2015; Liang et al., 2020; Huang et al., 2021).

important basis for forming depositional sequences, and a stratigraphic sequence corresponds to a cycle of change in stacking patterns, recorded as variation in lithological characteristics and logging curves (Catuneanu et al., 2009). In most cases, a single study of the sequence is insufficient for

determining the sequence interface. Therefore, critically integrating data from various sources is necessary (Zheng et al., 2000; Zheng et al., 2001). Moreover, unlike subaerial basins, no outcrops are found in the Mahu sag, and the sequence stratigraphic surfaces, such as weathering crusts,

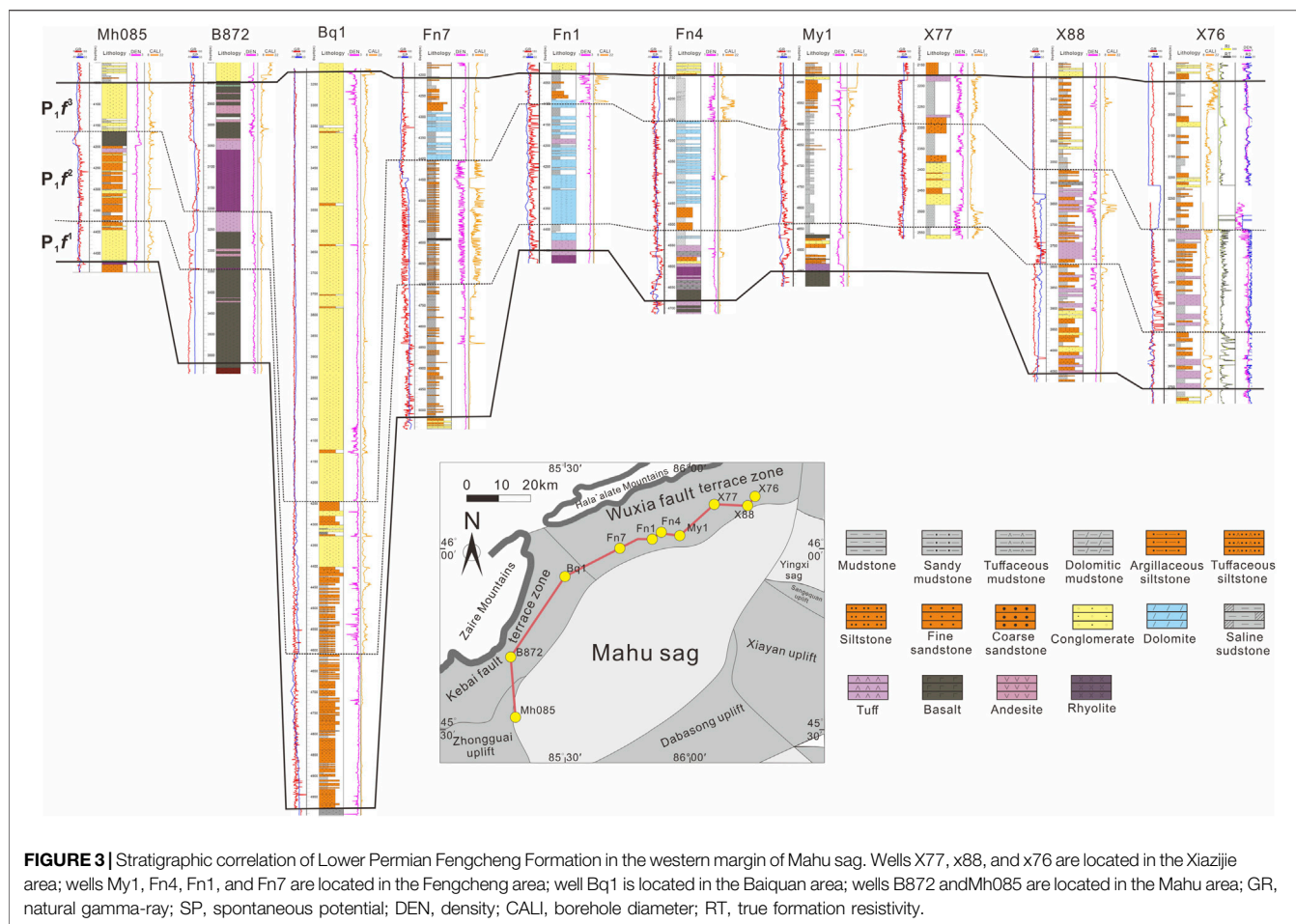


FIGURE 3 | Stratigraphic correlation of Lower Permian Fengcheng Formation in the western margin of Mahu sag. Wells X77, x88, and x76 are located in the Xiazijie area; wells My1, Fn4, Fn1, and Fn7 are located in the Fengcheng area; well Bq1 is located in the Baiquan area; wells B872 and Mh085 are located in the Mahu area; GR, natural gamma-ray; SP, spontaneous potential; DEN, density; CALL, borehole diameter; RT, true formation resistivity.

cannot be easily observed. Therefore, the stratigraphic sequence framework was determined by tracing and comparing the sequence boundaries based on the variations of logging curves (Van Wagoner et al., 1990; Miller et al., 2013; Zhu et al., 2017; Zou et al., 2020; Zou et al., 2021) and the contact relationships from cuttings and seismic data interpretation. Moreover, sedimentary facies are inferred from the observation of the drill cuttings and interpretation of the logging curves.

4 RESULTS

4.1 Stratigraphic Correlation

The Fengcheng Formation demonstrates an unconformable contact with the P_{1j} . The P_{1j} is composed of pyroclastic rock, andesite, and sandstone at the bottom and sandstone at the top, respectively (Figure 2). The overlying strata of P_{1f} is the P_{2x} . P_{1f} exhibits an unconformable contact with P_{2x} . Next, the P_{2x} is a set of gray-brown and brown-gray glutenite with a small amount of gray, brown-gray mudstone and sandstone.

The drilling of the Fengcheng Formation is distributed in the western margin of the Mahu sag, including the Xiazijie (wells X76, X88, X77, and X201), Fengcheng (wells Fn7, Fn4, Fn1, and

Fn7), Baiquan (Bq1), and Mahu areas (wells B872 and Mh085) (Figure 1D).

The P_{1f}^1 is composed of a gray, dark gray thin layer of tuff, dolomitic mudstone, and argillaceous dolomite near the sedimentary center; whereas, near the orogenic belt, tuff and siltstone are interbedded between thin layers glutenite, volcanic breccia, and basalt. Moreover, their logging curve shows high natural gamma ray (GR) and amplitude values, wave growth, and medium frequency (Figure 3).

The P_{1f}^2 is composed of deep gray and gray-black thin layers of muddy dolomite and dolomitic mudstone near the sedimentary center. Near the orogenic belt, it contains thin sandstone and mudstone interbedded between tuff and gravel. The logging curve of these rocks displays the following features: high-to-low GR values, high amplitude, short wavelength, and high frequency (Figure 3).

Next, the tuffaceous and dolomitic components of the P_{1f}^3 decrease; whereas, the sandy content increases. The bottom of the P_{1f}^3 is composed of mudstone and siltstone interbedded between dolomitic mudstone, whereas, its top is coarse sandstone and sandy conglomerate. The logging curve shows a low GR value, small amplitude, and continuous stability (Figure 3).



FIGURE 4 | Core photos of different lithology of Fengcheng Formation. **(A)** mudstone, plant leaf fossils can be seen on the cross section, well Mh39 at 5,269.68 m. **(B)** bituminous dolomitic mudstone with developed fractures and invaded by high concentration heavy oil, well F001 at 696.65 m. **(C)** fine sandy migmatite with a slightly thicker grain size and thin calcareous layer, well Fn1 at 4,421.85 m. **(D)** dolomitic siltstone, dolomitic strip filling can be seen on the boundary, local light under-invasion surface denudation dark top, dark part contains more dolomitic lenses, well Fn1 at 4,327 m. **(E)** dolomitic mudstone, see the crumpled structure. The dolomite is clumpy and irregularly laminated, well Fn011 at 3,862.8 m. **(F)** Fine sandy migmatite, well Fc011 well at 3,862.8 m. **(G)** tuffaceous gravel sandstone, well Fc011 well at 3,862.8 m. **(H)** breccia, well Bq5 at 3,575.4 m. **(I)** dark gray lava with accretionary volcanic gravel average particle size 1 cm, maximum particle size 2 cm, undeveloped stomata, well Md1 at 4,269 m. **(J)** basalt, undeveloped pores, and cryptocrystalline structure, well K204 at 4,375.0 m. **(K)** dolomitic gravel sandstone, coring depth, see the crumpled structure, well Ak1 at 5,666.8 m. **(L)** tuffaceous volcanic breccia, containing a large number of angular light-colored volcanic debris, well B872 at 3,250 m.

4.2 Sedimentary-Facies Analysis

During the sedimentation period of the Fengcheng Formation, the Mahu sag experienced complex tectonic activity, strong volcanic activity, and consequently formed various lithofacies. According to petrological characteristics and sedimentary structure, the sedimentary facies of the Fengcheng Formation are divided into two: lacustrine and fan–continental delta facies. Next, the lacustrine facies can be divided into semideep lake to deep lake and shore–shallow lake subfacies. The fan delta can be divided into fan–delta front subfacies and fan–delta plain subfacies.

4.2.1 Semideep Lake–Deep Lake Subfacies

The main lithofacies of semideep lake–deep lake subfacies are dark gray mudstone, gray–black mudstone, and gray–white dolomitic siltstone (Figures 4A–C). Semideep lake–deep lake subfacies are distributed in the Fengcheng area. Next, fossilized plant leaves can be seen in the dark gray mudstone (Figure 4A). In the F001 well, fissures in dolomitic mudstone are developed, and most of them are invaded by a high concentration of heavy oil (Figure 4B). In Fn1, light and dark dolomitic siltstone and dolomitic strip filling can be seen on the boundary. Moreover, the local light part under the invasion surface denudates the dark part, and the dark part contains more dolomitic lenses (Figure 4D).

4.2.2 Shore–Shallow Lake Subfacies

The shore–shallow lacustrine subfacies are distributed in most Mahu sag areas. The lithology is gray–white dolomitic mudstone, light gray–green fine sandy mixed rock, and gray–green mudstone. Next, soft-sedimentary deformation and folded structures are found in dolomitic mudstone (Figure 4E). Thin calcareous layers are present in gray–green fine sandy migmatite (Figure 4C). The gray–green mudstone contains several calcareous horizontal layers (Figure 4F). Wave sand ripple bedding, slump deformation structure, and antigrain sequence cycles are common in sand bodies.

4.2.3 Fan–Delta Facies

The fan delta refers to the fan body advancing from the adjacent mountain area to the stable water body, developed near the synsedimentary fault in the margin of the depression. The fan–delta front facies are composed of sandy conglomerate and dolomitic sandstone. The dolomitic sandstone exhibits a crumpled structure. Next, dolomite is clumpy and irregularly laminated. The grinding cycle of gravel is insufficient, and the gravel sorting is medium (Figure 4K). The subfacies rock types of fan–delta plain include fine, massive, and tuffaceous sand conglomerates (Figure 4H).

Sedimentary subfacies	Fan delta plain			Fan delta front		Lacustrine	Volcanic
Lithology	Glutenite			Dolomitic sandstone		Dolomite	Fused Tuff
	Finger glutenite	Massive glutenite	Tuffaceous glutenite				
Logging facies							
Seismic reflection characteristics							

FIGURE 5 | Characteristics of lithofacies seismic reflection and logging curve of Fengcheng Formation; GR, natural gamma curve; RT, true formation resistivity.

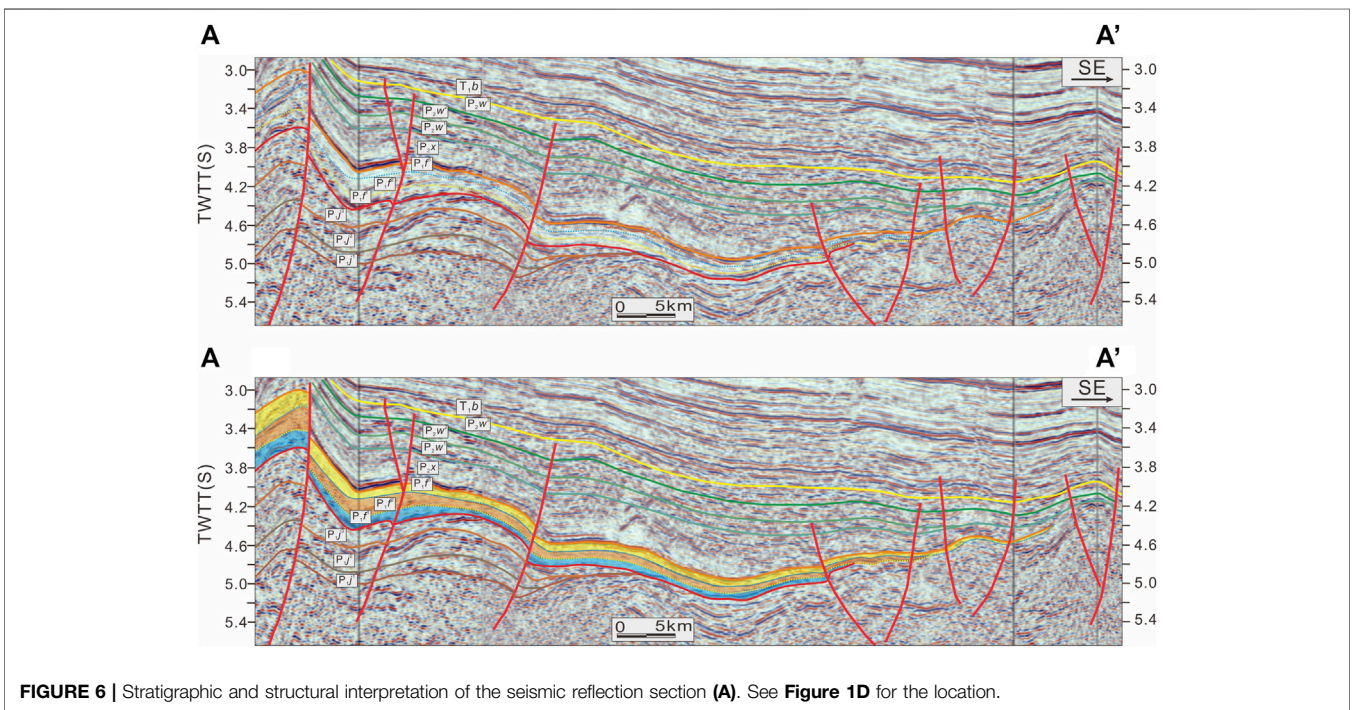


FIGURE 6 | Stratigraphic and structural interpretation of the seismic reflection section (A). See Figure 1D for the location.

4.2.4 Volcanic Facies

The volcanic rocks of P_1f^1 and P_1f^2 members are developed in the Mahu sag, containing massive molten gray breccia tuff, basalt, and volcanic breccia. The dark gray lava contains proliferated volcanic gravel, with an average particle size of 1 cm and a maximum particle size of 2 cm, with undeveloped pores (Figure 4I). The basalt demonstrated undeveloped stomata and a cryptocrystalline structure (Figure 4J). The surface section of the core was half-filled with white calcite. Light gray tuffaceous volcanic breccia contains several angular

light volcanic debris, demonstrating a matrix-support characteristic (Figure 4L).

4.3 Seismic Interpretation

Sections A and D–G are distributed from northwest to southeast, perpendicular to the extensional direction of the Mahu sag and the strike of the Kebai Fault (Figure 1D). Sections B and C are distributed in the northeast direction (Figure 1D).

The physical characteristics of sandy conglomerate, dolomitic sandstone, dolomitic mudstone, and volcanic

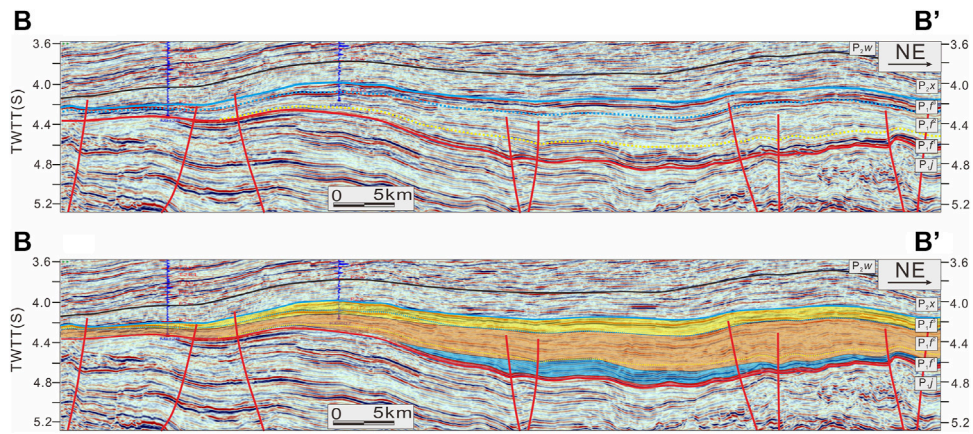


FIGURE 7 | Stratigraphic and structural interpretation of the seismic reflection section (B). See **Figure 1D** for the location.

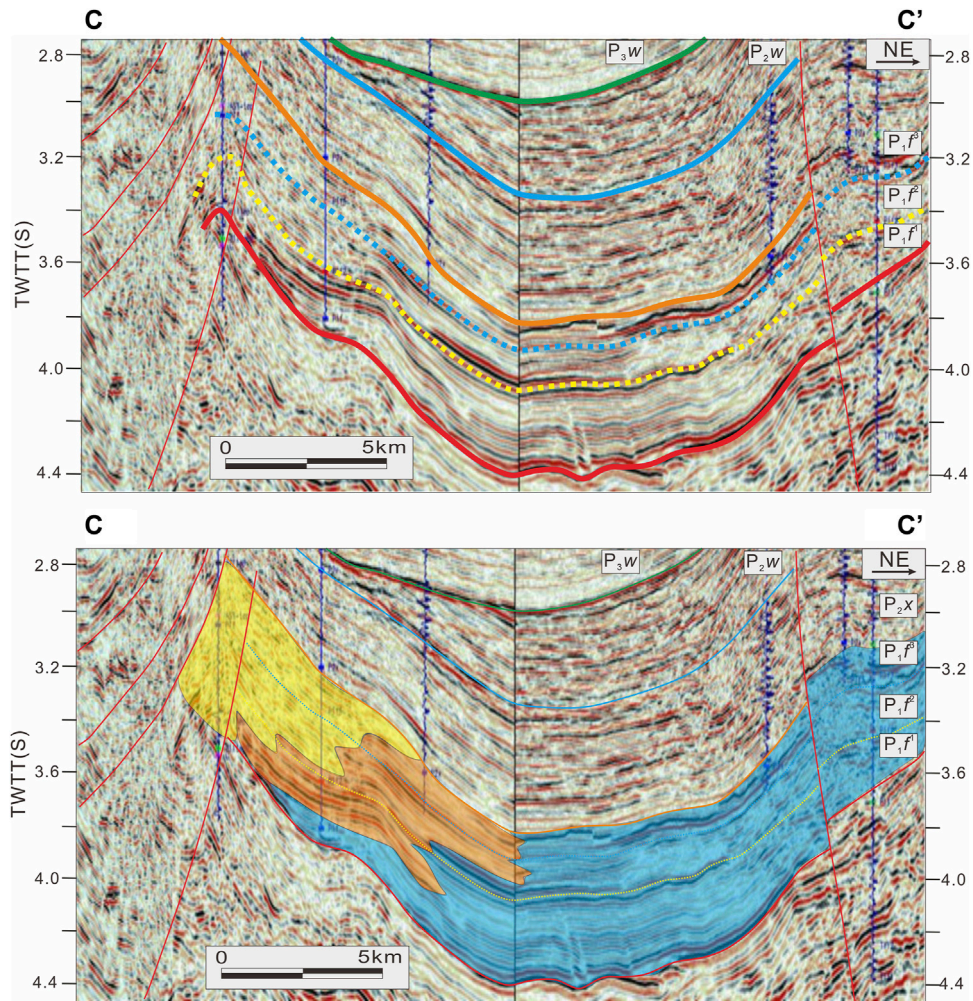


FIGURE 8 | Stratigraphic and structural interpretation of the seismic reflection section (C). See **Figure 1D** for the location. The legend is the same as **Figure 9**.

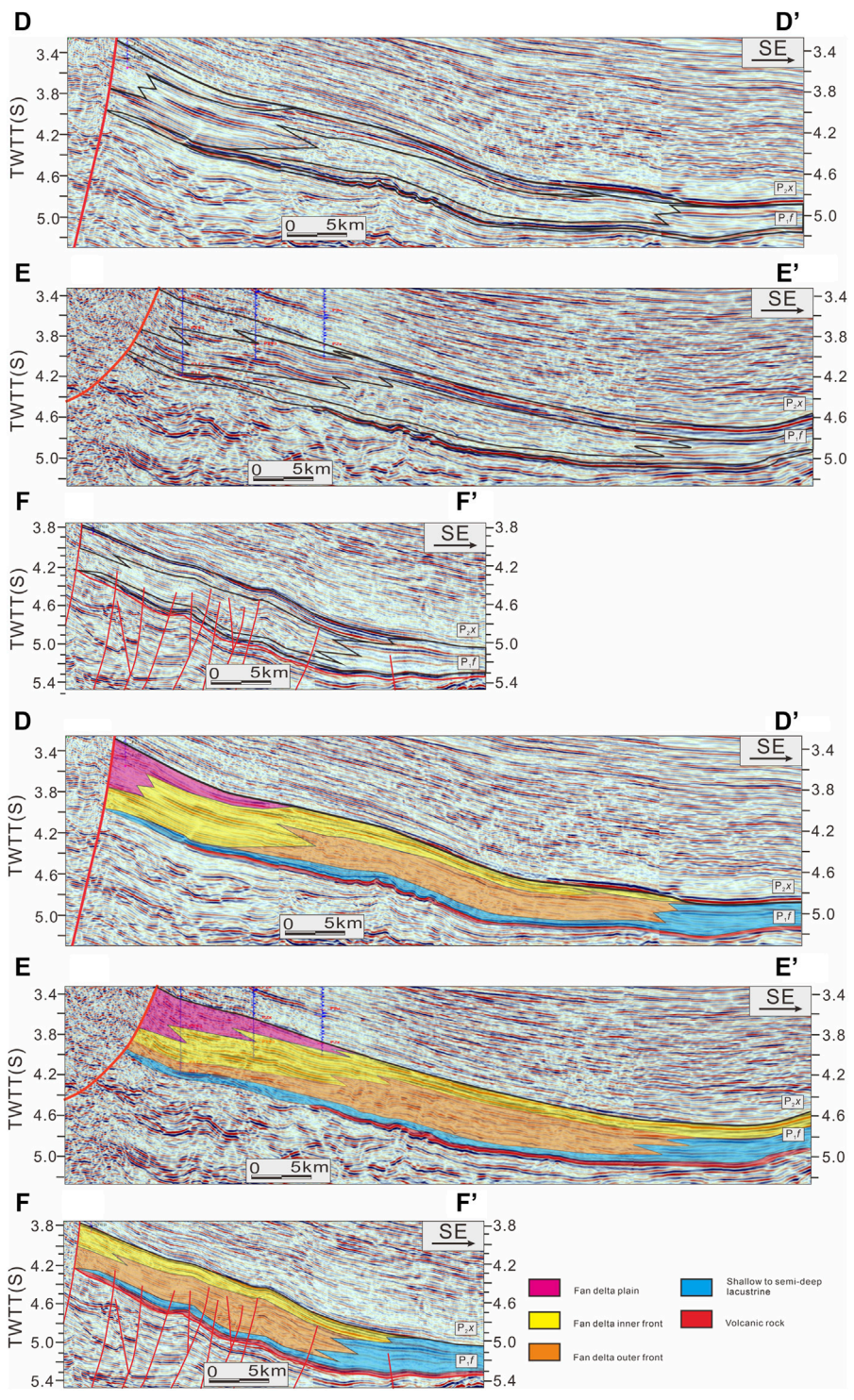


FIGURE 9 | Stratigraphic and structural interpretation of the seismic reflection section (D-F). See **Figure 1D** for the location.

rocks in the Fengcheng Formation are different, and they demonstrate apparent reflection characteristics in the seismic profiles (**Figure 5**). Different sedimentary facies correspond to different lithologic assemblages. Therefore,

combined with the logging curve, we identify four kinds of sedimentary facies on the seismic profile (**Figure 5**). The reflection characteristics of subsfacies' seismic profiles in fan-delta plain are medium and weak amplitude, poor

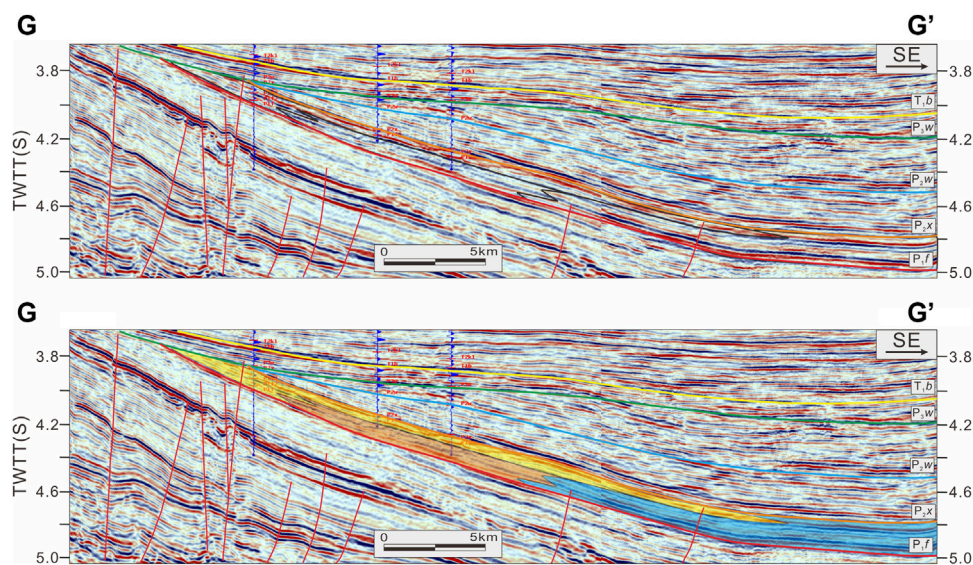


FIGURE 10 | Stratigraphic and structural interpretation of the seismic reflection section (G). See **Figure 1D** for the location. The legend is the same as **Figure 9**.

continuity, and disorderly reflection of medium and high frequencies (**Figure 5**). Next, the fan-delta front facies show low GR value, low true formation resistivity (RT) value, and straight curve in the logging facies. The seismic reflection of fan-delta front facies exhibits strong amplitude, good continuity, and medium- and low-frequency layered reflection (**Figure 5**). Volcanic rocks show good continuity, strong low-frequency reflection, and significant lateral differences in seismic profile (**Figure 5**).

Next, Section A is located north of the sag, extending from the Wuxia Fault to the entire Mahu sag up to the Xiayan uplift and extending 60 km. This section can identify the Permian strata in the study area and every member of the Fengcheng Formation. **Figure 6** shows the whole profile shape of the Fengcheng Formation, which deepens from the orogenic belt to the depression. Moreover, currently, the strata of the Fengcheng Formation are deformed by faults. The three members of the Fengcheng Formation overlap and pinch out layer by layer to the west edge of the lake basin, from top to bottom. The distribution of $P_1 f^3$ is the most extensive, followed by $P_1 f^2$ and $P_1 f^1$, respectively.

Section B (**Figure 7**) extends south to north along the sag's western margin and extends 80 km. This shows that the Fengcheng Formation in the north of the sag is thicker than that in the south. In addition, it also shows that the thickness of $P_1 f^2$ is more significant than those of $P_1 f^1$ and $P_1 f^3$.

Next, Section C is located in the Fengcheng area of the sag. Glutenite accumulates near the fault zone, and the range of lacustrine facies decreases from the $P_1 f^1$ to $P_1 f^3$ (**Figure 8**), showing the process of lake regression.

Then, Sections D, E, and F are located in the Huangyangquan fan in the central Mahu sag (**Figure 1D**) and identify the Fengcheng Formation fan-delta inner-front sand conglomerate, fan-delta outer-front sand gravel, and shallow

lake-semideep lacustrine dolomitic shale (**Figure 9**). Section G is located in the south of the sag, which can identify the glutenite in the inner front of the fan delta, glutenite in the outer front of the fan delta, and dolomitic mudstone of the shore-shallow lake (**Figure 10**). The sedimentary thickness of the south of the sag is thinner than that of the north, and the sand-conglomerate range of the inner front of the fan delta in the $P_1 f^3$ expands in the later stage. In addition, it shows that the outer-front dolomitic sandstone is covered with lacustrine mudstone (**Figure 10**).

4.4 Sequence Stratigraphy

4.4.1 Sequence Boundaries

The sequence boundary is defined by the contact relationship, which is revealed by the core, logging curve, and seismic profiles (**Figure 11**). Sequence boundary 1 (SB1) is the regional conformity between the $P_1 f^2$ and $P_1 f^3$ members of the Fengcheng Formation (**Figure 11**). SB1 appears at the bottom of the $P_1 f^3$, where large-scale alkaline evaporates and fan deltas are developed. The overall shape of the basal unconformity SB1 in the seismic profiles indicates a half-graben structure with NE-SW trending master faults (**Figure 6**). Sequence boundary 2 (SB2) is in the $P_1 f^3$.

The maximum flooding surfaces divide a backstepping retrogradational sequence pattern at the base from a progradational sequence pattern at the top (Catuneanu et al., 2009). Three maximum flooding surfaces (MFS) can be traced throughout the area, and they form the upper boundary for the transgressive system tracts (**Figures 11–13**). MFS is placed at the maximum GR response.

4.4.2 Sequence Stratigraphy Framework

The SQf1 is further divided into one expansion system tract (EST1) and two high-stand system tracts (HST1). The SQf2 and

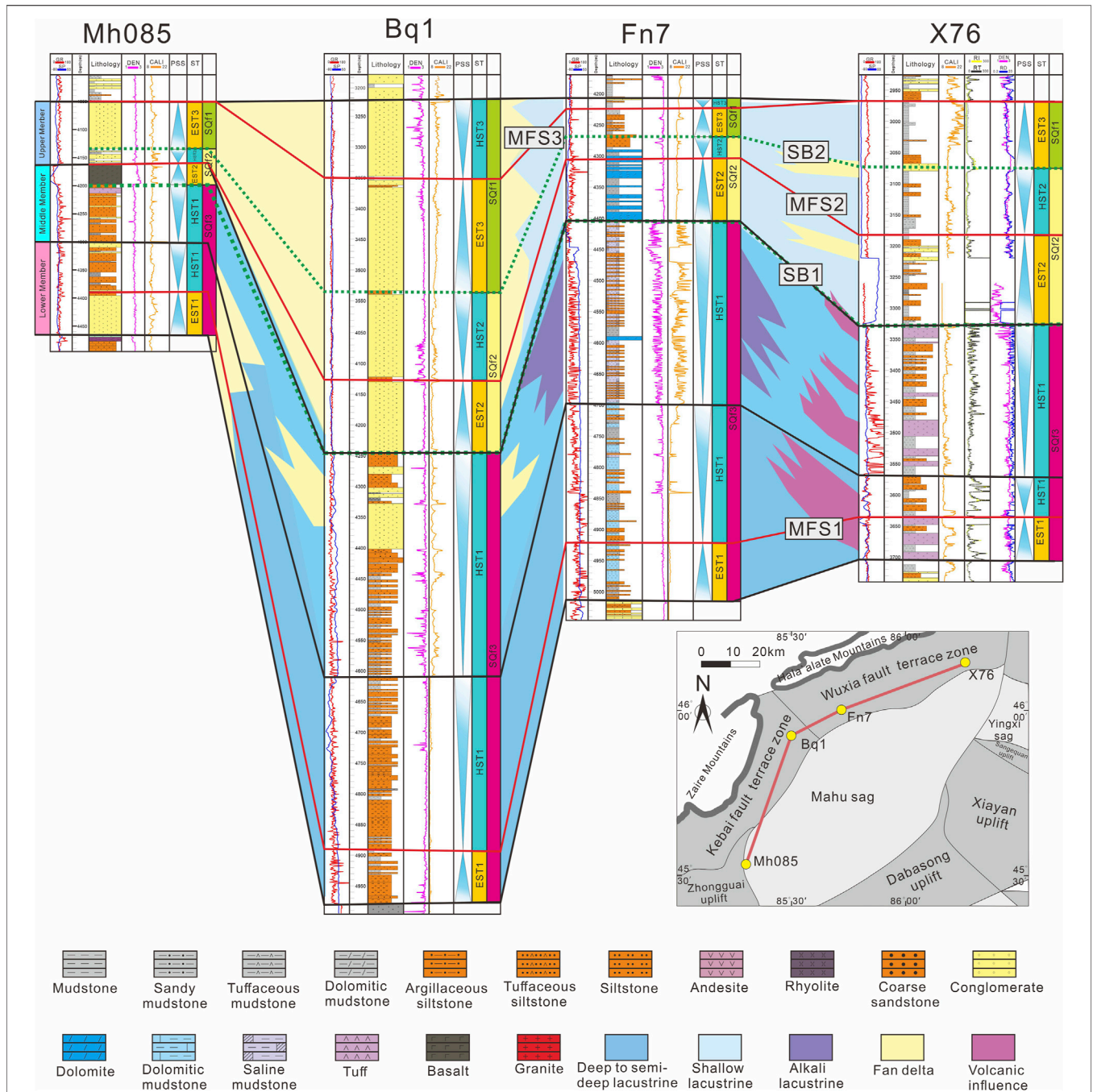


FIGURE 11 | The sequence stratigraphic connecting sections of wells X76, Fn7, Bq1, and Mh085 and the location of the well is shown in **Figure 1D**; PSS, parasequence set; ST, systems tract; EST, expansion system tract; HST, high-stand system tracts.

SQ3 are further divided into an expansion system tract (EST2 and EST3) and a high-stand system tract (HST2 and HST3).

EST1 is bounded above by MFS1. EST2 is bounded above and below by MFS2 and SB1, respectively. EST3 is bounded above and below by MFS3 and SB2, respectively (Figures 11–13). This unit comprises a retrogradational and fining-upward succession. In SQ1, EST1 is deposited in semideep lacustrine facies in the

Xiazijie, Fengcheng, and Baiquan areas; whereas, fan-delta front facies are in the Mahu area. Then, SQ2, SQ3, EST2, and EST3 are deposited as shallow lacustrine facies in Xiazijie, Fengcheng and the fan-delta facies in the Mahu and Baiquan areas. The units show lateral thickness variation, with the most significant thickness on the slope of the Fengcheng area.

HST1 is bounded below by MFS1 and above by SB1. HST2 is bounded below by MFS2 and above by SB2.

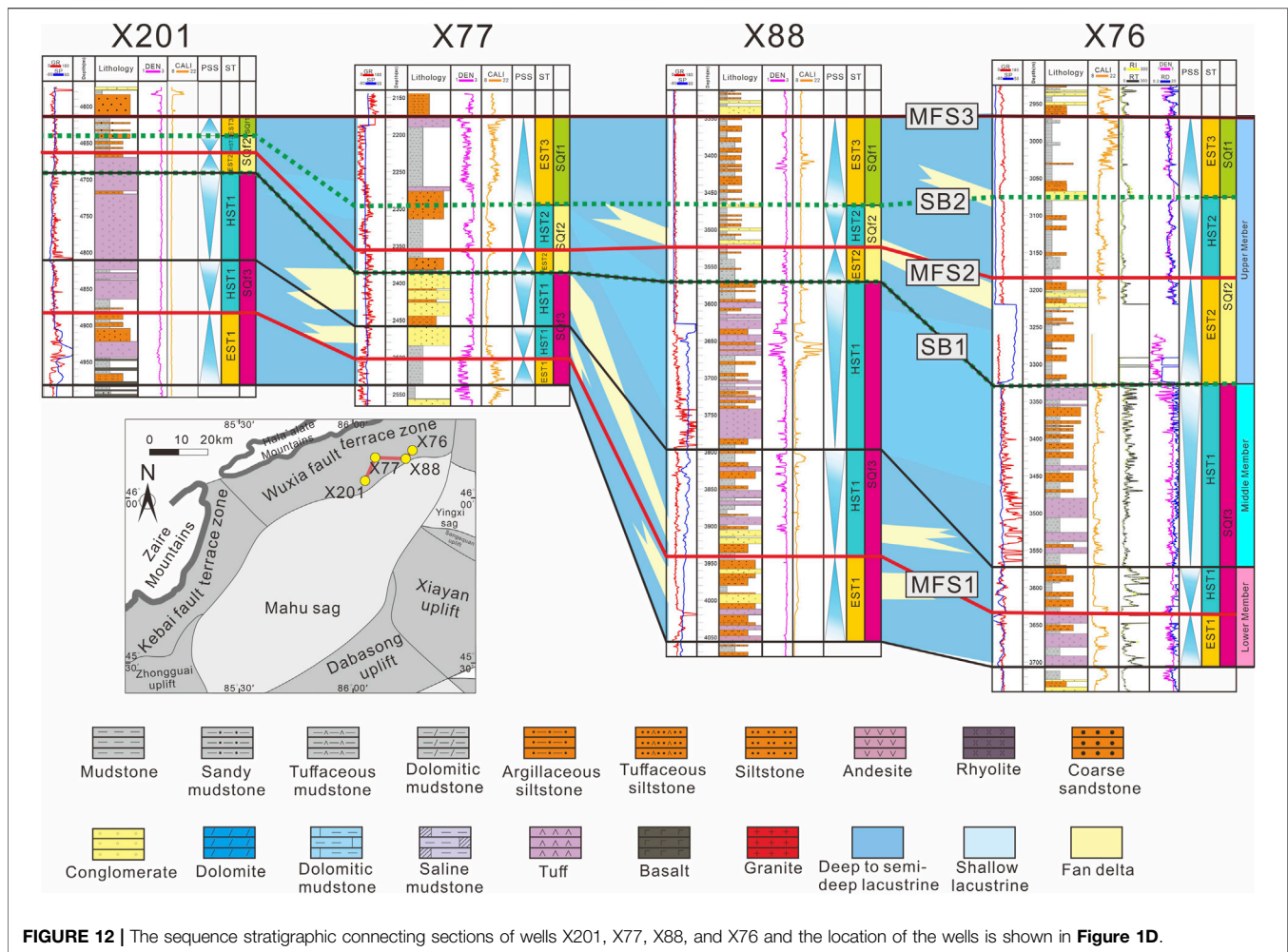


FIGURE 12 | The sequence stratigraphic connecting sections of wells X201, X77, X88, and X76 and the location of the wells is shown in **Figure 1D**.

HST3 is bounded below by MFS3 (**Figures 11–13**). HST1 is progradational, with a coarsening upward trend. In SQ1, HST1 is deposited near the alkaline lake, and more alkaline evaporite is distributed in the Fengcheng and Baiquan areas. The Xiazijie and Mahu areas are dominated by fan–delta front facies deposits. In SQ2 and SQ3, HST2 and HST3 are typical lacustrine deposits in the Fengnan and Xiazijie areas and thick fan–delta plain–facies deposits in the Baiquan and Mahu areas.

5 DISCUSSION

5.1 Sedimentary Evolution and Paleogeography

Through complete lithofacies' description and interpretation, stratigraphic sequence framework, and 2D seismic–reflection profile identification, we draw new lateral and vertical sedimentary–facies evolution maps of $P_1 f^1$, $P_1 f^2$, and $P_1 f^3$ in the Mahu sag (**Figure 14**). In addition, the potential provenances and transport routes of the Mahu sag were traced through previous provenance studies (Tang et al., 2020). These provide

necessary sedimentary face variations for the sedimentary–filling process described in this study.

During the sedimentary period of $P_1 f$ in the Xiazijie area, the lithology into pyroclastic deposits. $P_1 f^1$ is composed of tuff, followed by tuffaceous mudstone and siltstone. These sedimentary characteristics indicate that the Xiazijie area was in an evaporated shore–shallow lacustrine environment during the $P_1 f^1$. Next, volcanic activity was reduced as reflected in the decreased amount of tuff. At the beginning of $P_1 f^2$, the sedimentary grain size was reduced, and the content of tuffaceous rocks increased, indicating that the lake level rose, and volcanic activity increased. In $P_1 f^3$, little tuff and more sandy conglomerate is found, indicating that volcanic activity almost stopped, and the fan delta expanded. In the Xiazijie area, the provenance appears to be the Hala'ate mountains and volcanic materials in the Luliang uplift (Lu, 2018).

In the Fengcheng area, the bottom of $P_1 f^1$ contains limestone, mudstone, and sandstone, and the top of $P_1 f^1$ contains interbedded dolomitic mudstone and sandstone. This reflects that the $P_1 f^1$ is a semideep lake–deep lake environment with weak hydrodynamics and weak volcanic activity. In $P_1 f^2$, alkaline lacustrine deposits and salt-bearing mudstones reflect

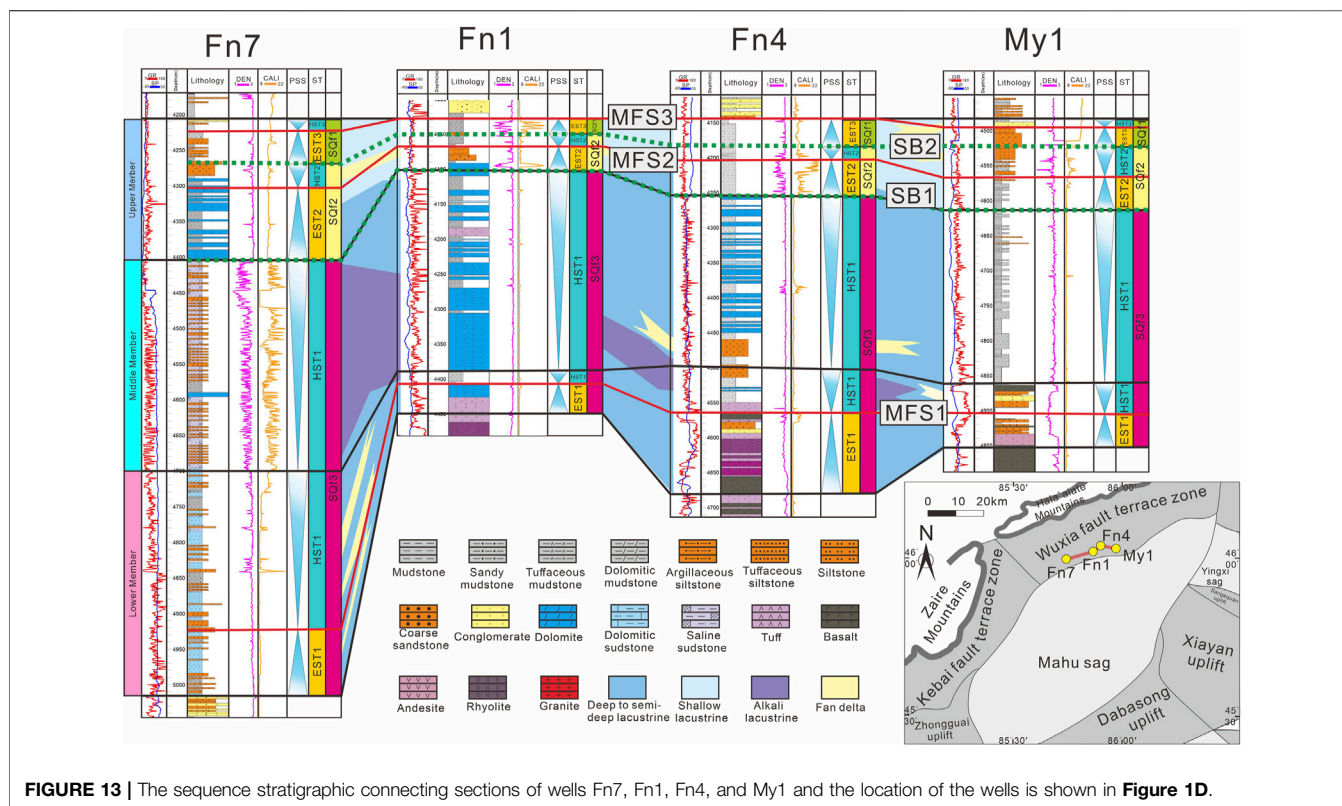


FIGURE 13 | The sequence stratigraphic connecting sections of wells Fn7, Fn1, Fn4, and My1 and the location of the wells is shown in **Figure 1D**.

a dry climate, with low-lake levels and high salinity that encouraged the formation of unique alkaline minerals. These alkaline minerals may be affected by deep hydrothermal fluids (Chang et al., 2016; Zhang et al., 2018; Tang et al., 2020). $P_1 f^3$ consists of lacustrine dolomite in the early stage and terrigenous clastic rock in the late stage, reflecting the decrease of lacustrine facies and the development of fan delta. It can be seen from Sections B (Figure 7) and C (Figure 8) that the Fengcheng area is the sedimentation center.

The Baiquan area is close to the Kebai fault zone and is located at the edge of the sedimentary lacustrine basin. $P_1 f^1$ is composed of dolomitic sandstone and a small amount of dolomitic mudstone. At the bottom of $P_1 f^2$, interbeds of cloud sand and mudstone are found, and the top is tuffaceous coarse sandstone. $P_1 f^3$ is a thick sandy conglomerate. Therefore, in $P_1 f^1$, the Baikouquan area is shore-shallow lacustrine facies. $P_1 f^2$ volcanic activity developed, and fan deltas began to develop. $P_1 f^3$ fan delta developed further. This is consistent with the change in sedimentary facies interpreted using the seismic profile. In Sections C–G (Figures 8–10), lacustrine deposits are deposited at the bottom of $P_1 f^1$, and a large area of lacustrine facies is transformed into fan-delta front facies within a short time. From $P_1 f^2$ to $P_1 f^3$, the fan-delta outer-front developed into the fan-delta inner front. In $P_1 f^3$, Sections D and E (Figure 9) develop fan-delta plain facies near the fault zone. Moreover, the provenance of the Baiquan area likely originated from the West Junggar block and Zaire mountains.

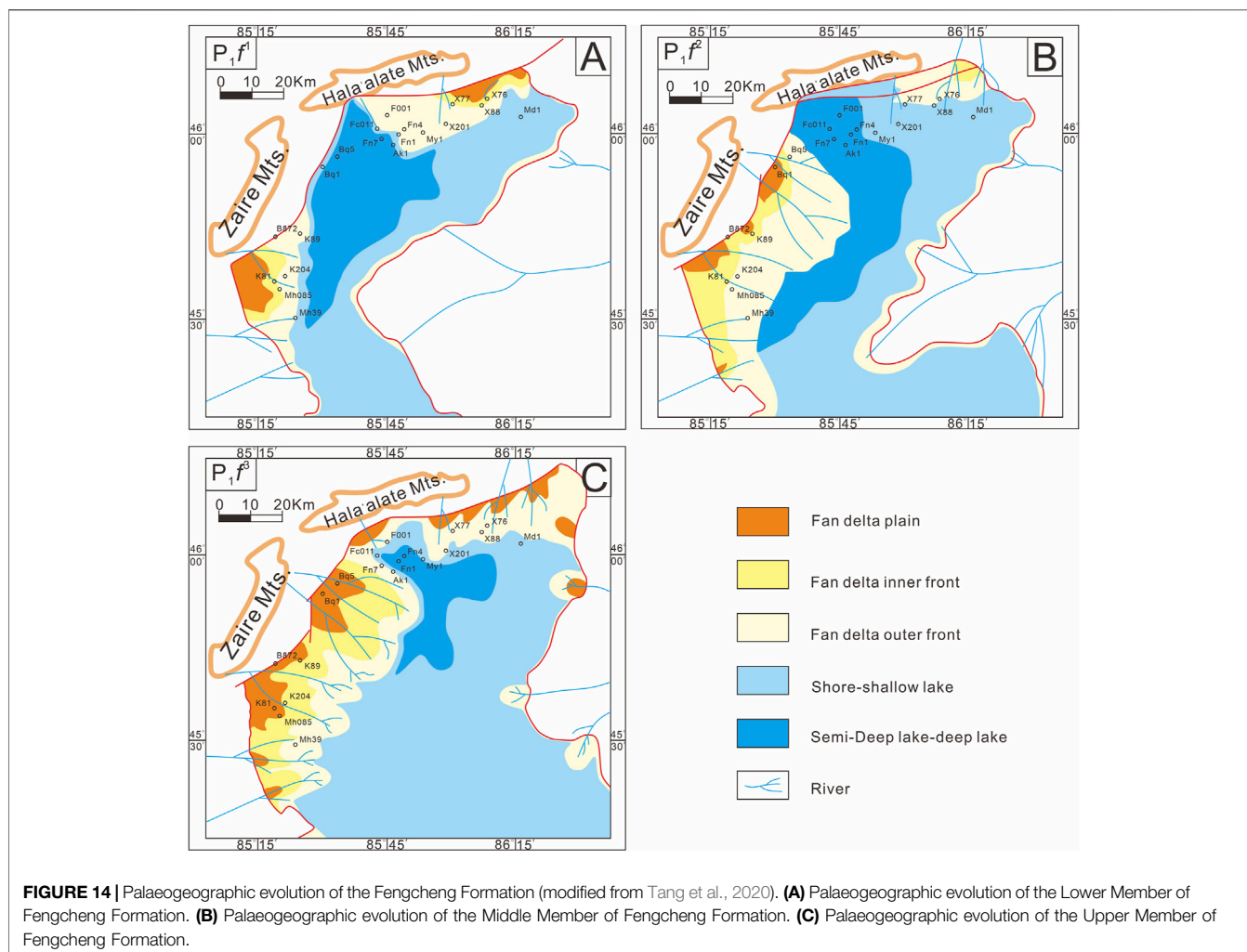
In the Mahu area, $P_1 f^1$ is deposited in shallow lacustrine facies. The tuffaceous sandy conglomerate is developed during

the early stage, and tuffaceous mudstone is developed in a low-energy environment. During the $P_1 f^2$ period, volcanic activity was frequent, and pyroclastic rocks were abundant. Volcanic rocks were developed at the top of $P_1 f^2$ in wells Mh085 (Figure 3). Therefore, the volcanic activity was intense during the deposition of upper $P_1 f^2$. During the deposition of $P_1 f^3$, the volcanic activity ceased, and the lake level dropped. The deposition is characterized by the fan-delta facies. Section G (Figure 10) shows that the sedimentary process of the Mahu area is similar to that of the Baiquan area. Thus, the fan delta was developed in the southern sag during the deposition of $P_1 f^2$ and $P_1 f^3$.

In summary, the $P_1 f^1$ deposition center was between the Baiquan and Fengcheng areas, and the lake reached its maximum depth. During this period, volcanic activity was frequent, and volcanic material provided part of the source. The fluvial delta deposits on the eastern slope originated from the Luliang uplift and flew through the river toward the center of the Mahu sag (Tang et al., 2021a). Next, during the deposition of $P_1 f^2$ and $P_1 f^3$, provenance increased in the southern Mahu and Baiquan areas, and fan deltas with a considerable thickness were developed (Figure 11). This provenance may come from the Zaire mountains.

5.2 Sediment-Filling Process and Sedimentary Model

Sections A and B (Figures 6 and 7) reflect the architecture of the Fengcheng Formation in the Mahu sag, which is deposited from the West Junggar terrane to the lake (Figure 1D). The distribution of the

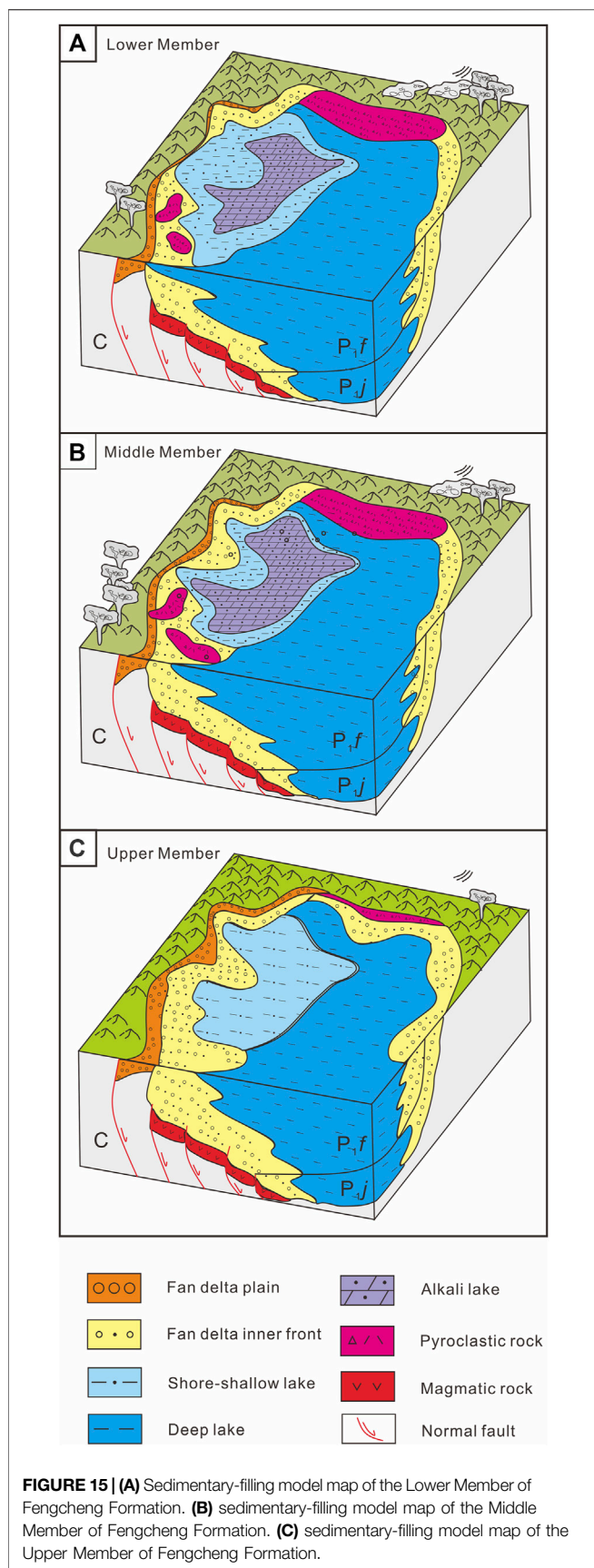


Fengcheng Formation in the north is controlled by paleogeomorphology and faults, and the depocenter is in the Fengcheng area of the Mahu sag. Moreover, the east–west seismic profile reveals that the characteristics of multiple half-graben structures in the lower Permian strata are pronounced (**Figure 6**). Unidirectional and single boundary faults control these structures. Next, the activity of the northwest-trending marginal–fault system in the late Permian led to the tectonic inversion of rift-related depressions in the early Permian (Liang et al., 2020). The half-graben structure and faulting style revealed by the seismic profiles (**Figure 6**), the paleogeographic reconstruction in the stratigraphic sequence framework (**Figure 11**), and the identification of soft-sediment deformation structures indicate that the early Permian Mahu sag was a rift basin (Yu et al., 2016; Liang et al., 2020; Tang et al., 2020; Tang et al., 2021a).

Figure 11 shows that P_1f^1 is a set of lacustrine deposits with its depocenter in the Fengcheng area, and only a small part of P_1f^1 was deposited in a fan–delta environment in the southern Mahu sag (**Figure 15A**). In P_1f^2 , the range of the lacustrine facies continues to expand (**Figure 15B**), and the area of the lake basin reaches the maximum (**Figure 11**). Tang et al. (2020) proposed that most of the soft-sediment deformation structures in P_1f^2 are caused by frequent

earthquakes, indicating basin-bounding normal fault activities in the depocenter, creating maximal accommodation. Next, geochemical data and alkaline minerals show that the P_1f^2 member of the Mahu sag is an alkaline lake basin with high salinity (Gong et al., 2014; Cao et al., 2015; Zhang et al., 2018). At the beginning of the deposition of P_1f^3 , the range of lacustrine facies shrinks, and the Xiazijie and Fengcheng areas are shore–shallow lacustrine deposits. The Baiquan and Mahu areas were the fan–delta facies’ deposits, and the lake basin began to shrink (**Figure 15C**).

During the syn-rift stage of a rift basin, due to gravity isostasy, the continuous subsidence of the half-graben will lead to the uplift of the horst, increasing the sedimentary supply from the proximal horst sources (Chao et al., 2021). Based on the detrital zircon U–Pb chronology of the Fengcheng Formation, Tang et al. (2021c) demonstrated a transition from distant axial provenance areas to proximal lateral horsts in West Junggar during the syn-rifting processes in the Mahu sag. Next, Sections C–F (**Figures 8 and 9**) in the Baikouquan area and Section G (**Figure 10**) in the Mahu area show different filling processes in the margin of the basin. In the Baiquan area, fan–delta sequences accumulate toward the depocenter in the Mahu sag (**Figures 8 and 9**). The rock grain size became coarser and evolved from lacustrine facies to fan–delta



front facies in $P_1 f^1$ and $P_1 f^2$ and finally to fan–delta plain facies in $P_1 f^3$, suggesting that the rate of sedimentary supply is higher than subsidence, which is consistent with the filling processes in the margin of a rift basin.

Therefore, the sediment-filling process of the Fengcheng Formation is controlled by fault activity. The Fengcheng Formation experienced a lake-basin expansion during the deposition of $P_1 f^1$ and $P_1 f^2$ and a shrinkage stage during the deposition of $P_1 f^3$ (Figure 15).

6 CONCLUSION

The Fengcheng Formation consists of three third-order sequence stratigraphy (SQf1, SQf2, and SQf3). The SQf1 is divided into one expansion system tract (EST1) and two high-stand system tracts (HST1). The SQf2 consists of EST2 and HST2. The SQf3 consists of EST3 and HST3. In SQf1, EST1 was deposited in semideep lacustrine facies in the Xiazijie, Fengcheng, and Baiquan areas. Fan–delta front facies are in the Mahu area, HST1 is deposited near the alkaline lake, and more alkaline evaporite is distributed in the Fengcheng and Baiquan areas. The Xiazijie and Mahu areas are dominated by fan–delta front facies deposits. In SQf2 and SQf3, EST2 and EST3 were deposited as shallow lacustrine facies in Xiazijie and Fengcheng and fan–delta facies in the Mahu and Baiquan areas; HST2 and HST3 are typical lacustrine deposits in the Fengcheng and Xiazijie areas and thick fan–delta plain–facies deposits in the Baiquan and Mahu areas.

The deposition center was between the Baiquan and Fengcheng areas. During the sedimentary period of $P_1 f^1$ and $P_1 f^2$, volcanic activity was frequent, and volcanic material provided part of the source. During the deposition of $P_1 f^2$ and $P_1 f^3$, provenance increased in the southern Mahu and Baiquan areas and developed fan delta.

The sedimentary-filling model of the Fengcheng Formation in Mahu sag is controlled by the fault. Next, the lake basin of the Mahu sag experienced a sedimentary-filling process from the expansion of $P_1 f^1$ and $P_1 f^2$ to the contraction of $P_1 f^3$. Sedimentary supply rate at the margin of Mahu sag is higher than subsidence, which is consistent with the filling processes at the margin of a rift basin.

DATA AVAILABILITY STATEMENT

The original contributions presented in the study are included in the article/supplementary material; further inquiries can be directed to the corresponding authors.

AUTHOR CONTRIBUTIONS

WT and ML are responsible for writing and drawing, while XC, CH, NS, WT, and ZQ are responsible for content revision and sample collection. DZ and DG are responsible for the review of the content of the article.

FUNDING

This research is supported by the Chinese National Natural Science Foundation (No. 41802177), the Prospective and Fundamental Project of PetroChina (2021DJ0206), and the Fund for Basic Science Research of PetroChina (2020D-5008-04).

REFERENCES

- Cao, J., Hu, W. X., Yao, S. P., Zhang, Y. J., Wang, X. L., Zhang, Y. Q., et al. (2006). Evolution of Petroleum Migration and Accumulation in the Northwestern Margin of the Junggar Basin Fluid Inclusion Geochemistry. *Geol. Rev.* 2006 (05), 700–707. doi:10.16509/j.georeview.2006.05.023
- Cao, J., Lei, D. W., Li, Y. W., Tang, Y., Wang, T., Chang, Q. S., et al. (2015). Ancient High-Quality Alkaline Lacustrine Source Rocks Discovered in the Lower Permian Fengcheng Formation, Junggar Basin. *Acta Pet. Sin.* 36 (07), 781–790. doi:10.7623/syxb201507002
- Carroll, A. R., Graham, S. A., Hendrix, M. S., Ying, D., and Zhou, D. (1995). Late Paleozoic Tectonic Amalgamation of Northwestern China: Sedimentary Record of the Northern Tarim, Northwestern Turpan, and Southern Junggar Basins. *Geol. Soc. Am. Bull.* 107, 571–594. doi:10.1130/0016-7606(1995)107<0571:lptaon>2.3.co;2
- Catuneanu, O., Abreu, V., Bhattacharya, J. P., Blum, M. D., Dalrymple, R. W., Eriksson, P. G., et al. (2009). Towards the Standardization of Sequence Stratigraphy. *Earth-Sci. Rev.* 92 (1), 1–33. doi:10.1016/j.earscirev.2008.10.003
- Chang, H. L., Zheng, R. C., Guo, C. L., and Wen, H. G. (2016). Characteristics of Rare Earth Elements of Exhalative Rock in Fengcheng Formation, Northwestern Margin of Junggar Basin. *Geol. Rev.* 62 (03), 550
- Chao, D., Zhu, R. X., Han, J. H., Shu, Y., Wu, Y. X., Hou, K. F., et al. (2021). Impact of Basement Thrust Faults on Low-Angle Normal Faults and Rift Basin Evolution: a Case Study in the Enping Sag, Pearl River Basin. *Solid earth.* 12, 2327–2350. doi:10.5194/se-12-2327-2021
- Chen, J. F., Han, B. F., Ji, J. Q., Zhang, L., Xu, Z., He, G. Q., et al. (2010). Zircon U–Pb Ages and Tectonic Implications of Paleozoic Plutons in Northern West Junggar, North Xinjiang, China. *Lithos* 115 (1–4), 137–152. doi:10.1016/j.lithos.2009.11.014
- Fang, X., Yang, Z., Yan, W., Guo, X., Wu, Y., and Liu, J. (2019). Classification Evaluation Criteria and Exploration Potential of Tight Oil Resources in Key Basins of China. *J. Nat. Gas Geoscience* 4 (6), 309–319. doi:10.1016/j.jnggs.2019.11.002
- Feng, C., Lei, D., Qu, J., and Huo, J. (2019). Controls of Paleo-Overpressure, Faults and Sedimentary Facies on the Distribution of the High Pressure and High Production Oil Pools in the Lower Triassic Baikouquan Formation of the Mahu Sag, Junggar Basin, China. *J. Petroleum Sci. Eng.* 176, 232–248. doi:10.1016/j.petrol.2019.01.012
- Gong, B. S., Wen, H. G., Li, C. L., Wang, L., Zheng, R. C., and Qi, L. Q. (2014). Sedimentary Environment of Fengcheng Formation in Urho Area, Junggar Basin. *Lithol. Reserv.* 26 (02), 59
- Gong, D., Li, J., Ablimit, I., He, W., Lu, S., Liu, D., et al. (2018). Geochemical Characteristics of Natural Gases Related to Late Paleozoic Coal Measures in China. *Mar. Petroleum Geol.* 96, 474–500. doi:10.1016/j.marpetgeo.2018.06.017
- Gong, D. Y., Wang, X. L., Zhou, C. M., Chen, G., Wu, W. A., and Liu, Y. H. (2020). Hydrocarbon Generation Potential of Middle Triassic Karamay Formation in the Northwestern Junggar Basin. *J. China U Min. Techno* 49 (2), 328
- Gong, D. Y., Zhang, Y. Q., Guo, W. J., Song, Z. H., Lu, S., and Wu, W. S. (2019). The Identification of Secondary Microbial Methane and biodegradation: Case Study of Luliang Oil and Gas Field, Junggar Basin. *Nat. Gas. Geosci.* 30 (7), 1006
- Han, B.-F., Guo, Z.-J., Zhang, Z.-C., Zhang, L., Chen, J.-F., and Song, B. (2010). Age, Geochemistry, and Tectonic Implications of a Late Paleozoic Stitching Pluton in the North Tian Shan Suture Zone, Western China. *Geol. Soc. Am. Bull.* 122, 627–640. doi:10.1130/b26491.1
- He, D. F., Yin, C., Du, S. K., Shi, X., and Ma, H. S. (2004b). Characteristics of Structural Segmentation of Foreland Thrust Belts—A Case Study of the Fault Belts in the Northwestern Margin of Junggar Basin. *Earth Sci. Front.* (03), 91
- He, D. F., Zhang, L., Wu, S. T., Li, D., and Zhen, Y. (2018). Tectonic Evolution Stages and Features of the Junggar Basin. *Oil Gas. Geol.* 39 (5), 845–861. doi:10.11743/ogg20180501
- He, G. Q., Chen, S. D., Xu, X., Li, J. Y., and Hao, J. (2004a). *An Introduction to Tectonic Map of Xinjiang and its Neighboring Area (1: 250 000)*. Beijing: Geological Publishing House, 65.
- Hendrix, M. S., Graham, S. A., Carroll, A. R., Sobel, E. R., McKnight, C. L., Schuelein, B. J., et al. (1992). Sedimentary Record and Climatic Implications of Recurrent Deformation in the Tian Shan: Evidence from Mesozoic Strata of the North Tarim, South Junggar, and Turpan Basins, Northwest China. *Geol. Soc. Am. Bull.* 104, 53–79. doi:10.1130/0016-7606(1992)104<0053:sracio>2.3.co;2
- Huang, H., Gao, Y., Ma, C., Niu, L., Dong, T., Tian, X., et al. (2021). Astronomical Constraints on the Development of Alkaline Lake during the Carboniferous–Permian Period in North Pangea. *Glob. Planet. Change* 207, 103681. doi:10.1016/j.gloplacha.2021.103681
- Jia, F. J., Yao, W. J., Liang, Z. L., Zhang, S. C., Fang, L. H., and Shi, J. A. (2010). Diagenetic Feature and Evolution of Reservoir Pore of Permian Reservoir under the Kebai Fault in the Northwestern Margin Junggar Basin. *Nat. Gas. Geosci.* 21 (03), 458–463. doi:10.1016/j.petrol.2020.107599
- Kuang, J., and Qi, X. F. (2006). The Structural Characteristics and Oil-Gas Explorative Direction in Junggar Foreland Basin. *Xinjiang Pet. Geol.* 2006 (01), 5
- Lei, D. W., Abulimiti, B., Tang, Y., Chen, J., and Cao, J. (2014). Controlling Factors and Occurrence Prediction of High Oil-Gas Production Zones in Lower Triassic Baikouquan Formation of Mahu Sag in Junggar Basin. *Xinjiang Pet. Geol.* 35 (05), 495
- Lei, Z. Y., Lu, B., Wei, Y. J., Zhang, L. P., and Shi, X. (2005). Tectonic Evolution and Development and Distribution of Fans on Northwestern Edge of Junggar Basin. *Oil Gas. Geol.* (01), 86. doi:10.3969/j.issn.1001-3873.2006.01.002
- Li, L. (2022). Development of Natural Gas Industry in China: Review and Prospect. *Nat. Gas. Ind. B* 9 (2), 187–196. doi:10.1016/j.ngib.2022.03.001
- Li, W., Yu, Z., Wang, X., Yu, Z., Lu, X., and Feng, Q. (2020). Formation Mechanisms of Deep and Ultra-deep over Pressure Caprocks and Their Relationships with Super-large Gas Fields in the Petroliiferous Basins of China. *Nat. Gas. Ind. B* 7 (5), 443–452. doi:10.1016/j.ngib.2020.09.002
- Li, Y., Xu, Q., Liu, J., Wang, R., and Xiang, K. (2016). Redefinition and Geological Significance of Jiamuhe Formation in Hala’alate Mountain of West Junggar, Xinjiang. *Earth Sci.* 41 (09), 147–1488. doi:10.3799/dqkx.2016.516
- Liang, Y., Zhang, Y., Chen, S., Guo, Z., and Tang, W. (2020). Controls of a Strike-Slip Fault System on the Tectonic Inversion of the Mahu Depression at the Northwestern Margin of the Junggar Basin, NW China. *J. Asian Earth Sci.* 198, 104229. doi:10.1016/j.jseas.2020.104229
- Liu, M., Zhang, S. C., Kong, Y. H., and Shi, J. A. (2013). The Sedimentary Facies Research of Fengcheng Formation of Permian in Fengcheng Area, the Northwestern Margin of Junggar Basin. *Xinjiang Geol.* 31 (03), 236
- Lu, X., Sun, D., Xie, X., Chen, X., Zhang, S., Zhang, S., et al. (2019). Microfacies Characteristics and Reservoir Potential of Triassic Baikouquan Formation, Northern Mahu Sag, Junggar Basin, NW China. *J. Nat. Gas Geoscience* 4 (1), 47–62. doi:10.1016/j.jnggs.2019.03.001
- Lu, Y. (2018). *Permian Chronostratigraphic Framework and Sedimentary Filling Evolution in Mahu-Shawan and Adjacent Area, Junggar Basin [Master Thesis]*. Beijing: China University of Geosciences Beijing, 132.
- Miller, K. G., Browning, J. V., Mountain, S. G., Bassetti, M. A., Monteverde, D., Katz, M. E., et al. (2013). Sequence Boundaries Are Impedance Contrasts: Core-Seismic-Log Integration of Oligocene–Miocene Sequences, New Jersey Shallow Shelf. *Geosphere* 9 (5), 1257–1285. doi:10.1130/GES00858.1
- Niu, H. Q., Chen, S. Y., Zhang, P., and Yan, J. H. (2009). Analysis of the Permian Reservoir Characteristics and Controlling Factors in Wuxia Area, Junggar Basin. *J. Palaeogeogr.* 1 (4), 425–434. doi:10.7605/gdxb.2009.04.007

ACKNOWLEDGMENTS

We thank the editor-in-chief and the two reviewers for their constructive comments and careful corrections that led to significant improvement of the manuscript. We thank Xinjiang Oilfield, China National Petroleum Corporation for providing drill cores, wireline logs and seismic profiles.

- Ouyang, Y., Tian, W., Sun, B., Wang, B., Qi, L., Sun, Q., et al. (2018). Accumulation Characteristics and Exploration Strategies of Coal Measure Gas in China. *Nat. Gas. Ind. B* 5 (5), 444–451. doi:10.1016/j.ngib.2018.03.003
- Pei, L., Gang, W., Zhu, C., Liu, Y., He, W., Dong, Y., et al. (2018). Carbon Isotope and Origin of the Hydrocarbon Gases in the Junggar Basin, China. *J. Nat. Gas Geoscience* 3 (5), 253–261. doi:10.1016/j.jnggs.2018.11.002
- Shi, J. a., Sun, G., Zhang, S., Guo, H., Zhang, S., and Du, S. (2017). Reservoir Characteristics and Control Factors of Carboniferous Volcanic Gas Reservoirs in the Dixi Area of Junggar Basin, China. *J. Nat. Gas Geoscience* 2 (1), 43–55. doi:10.1016/j.jnggs.2017.03.001
- Tang, W. B., Song, Y., He, W. J., Tang, Y., Guo, X. G., Pe-Piper, G., et al. (2021a). Source-to-sink Evolution of Syn-Rift Alkaline Lake Sediments in the Lower Permian Fengcheng Formation, Junggar Basin, NW China: Evidence from Petrology, Detrital Zircon Geochronology and Geochemistry. *J. Asian Earth Sci.* 232, 105049. doi:10.1016/j.jseae.2021.105049
- Tang, W., Zhang, Y., Pe-Piper, G., Piper, D. J. W., Guo, Z., and Li, W. (2021c). Permian Rifting Processes in the NW Junggar Basin, China: Implications for the Post-accretionary Successor Basins. *Gondwana Res.* 98, 107–124. doi:10.1016/j.gr.2021.06.005
- Tang, W., Zhang, Y., Pe-Piper, G., Piper, D. J. W., Guo, Z., and Li, W. (2021b). Permian to Early Triassic Tectono-Sedimentary Evolution of the Mahu Sag, Junggar Basin, Western China: Sedimentological Implications of the Transition from Rifting to Tectonic Inversion. *Mar. Petroleum Geol.* 123, 104730. doi:10.1016/j.marpetgeo.2020.104730
- Tang, W., Zhang, Y., Pe-Piper, G., Piper, D. J. W., Guo, Z., and Li, W. (2020). Soft-sediment Deformation Structures in Alkaline Lake Deposits of Lower Permian Fengcheng Formation, Junggar Basin, NW China: Implications for Syn-Sedimentary Tectonic Activity. *Sediment. Geol.* 406, 105719. doi:10.1016/j.sedgelo.2020.105719
- Vail, P. R. (1988). *AAPG Annual Convention Short Course: Sequence Stratigraphy Interpretation of Seismic Stratigraphy Interpretation Procedure*. Houston, TX: AAPG Bull.-Am. Assoc. Petr.
- Van Wagoner, J. C., Mitchum, R. M., and Campion, K. M. (1990). "Siliciclastic Sequence Stratigraphy in Well Logs, Cores and Outcrops," in *American Association of Petroleum Geologists Methods in Exploration Series*. Editors J. Helwig and G. D. Howell (Oklahoma, OK: AAPG Bull.-Am. Assoc. Petr. Geol.), 7, 2–8. doi:10.1306/mth7510
- Wang, Y., Jia, D., Pan, J., Wei, D., Tang, Y., Wang, G., et al. (2018). Multiple-phase Tectonic Superposition and Reworking in the Junggar Basin of Northwestern China-Implications for Deep-Seated Petroleum Exploration. *Bulletin* 102, 1489–1521. doi:10.1306/10181716518
- Wei, G., Li, J., She, Y., Zhang, G., Shao, L., Yang, G., et al. (2018). Distribution Laws of Large Gas Fields and Further Exploration Orientation and Targets in China. *Nat. Gas. Ind. B* 5 (5), 485–498. doi:10.1016/j.ngib.2018.04.014
- Xian, J. Y. (1985). Discussion on Rock Ore and Reservoir Characteristics of Fengcheng Formation in Fengcheng Area. *Xinjiang Pet. Geol.* (03), 28
- Yu, Y., Wang, X., Rao, G., and Wang, R. (2016). Mesozoic Reactivated Transpressional Structures and Multi-Stage Tectonic Deformation along the Hong-Che Fault Zone in the Northwestern Junggar Basin, NW China. *Tectonophysics* 679, 156–168. doi:10.1016/j.tecto.2016.04.039
- Zhang, G., Jin, L., Lan, L., and Zhao, Z. (2015). Analysis of the Orderly Distribution of Oil and Gas Fields in China Based on the Theory of Co-control of Source and Heat. *Nat. Gas. Ind. B* 2 (1), 49–76. doi:10.1016/j.ngib.2015.02.005
- Zhang, S. W. (2013). Identification and its Petroleum Geologic Significance of the Fengcheng Formation Source Rocks in Hala' Alt Area, the Northern Margin of Junggar Basin. *Oil Gas. Geol.* 34 (02), 145. doi:10.11743/ogg20130201
- Zhang, S., Zhang, S., Fang, L., Lu, X., Guo, H., and Shi, J. a. (2020). Petrological and Geochemical Constraints on Tectonic Settings of the Late Carboniferous-Early Permian, Central Junggar, China. *J. Nat. Gas Geoscience* 5 (1), 1–10. doi:10.1016/j.jnggs.2019.12.002
- Zhang, Y. J., Cao, J., and Hu, W. X. (2010). Timing of Petroleum Accumulation and the Division of Reservoir-Forming Assemblages, Junggar Basin, NW China. *Pet. Explor. Dev.* 37 (03), 257–262. doi:10.1016/S1876-3804(10)60031-6
- Zhang, Z. J., Yuan, X. J., Wang, M. S., Zhou, C. M., Tang, Y., Chen, X. Y., et al. (2018). Alkaline-lacustrine Deposition and Paleoenvironmental Evolution in Permian Fengcheng Formation at the Mahu Sag, Junggar Basin, NW China. *Pet. Explor. Dev.* 45 (06), 972–984. doi:10.1016/s1876-3804(18)30107-1
- Zheng, R. C., Peng, J., and Wu, C. R. (2001). Grade Divisions of Base-Level Cycle of Terrigenous Basin and its Implications. *Acta Sedimentol. Sin.* 2, 249
- Zheng, R. C., Wu, C. R., and Ye, M. C. (2000). Research Think of Highresolution Sequence Stratigraphy about a Sterrigenous Basin. *J. Chengdu Univ. Technol. Sci. Ed.* 3, 241
- Zhi, D. M., Song, Y., He, W. J., Jia, X. Y., Zou, Y., and Huang, L. L. (2019). Geological Characteristics, Resource Potential and Exploration Direction of Shale Oil in Middle-Lower Permian, Junggar Basin. *Xinjiang Pet. Geol.* 40 (04), 389–401. doi:10.7657/XJPG20190402
- Zhi, D. M., Tang, Y., He, W. J., Guo, X. G., Zheng, M. L., and Huang, L. L. (2021). Orderly Coexistence and Accumulation Models of Conventional and Unconventional Hydrocarbons in Lower Permian Fengcheng Formation, Mahu Sag, Junggar Basin. *Pet. Explor. Dev.* 48 (01), 38–51. doi:10.1016/s1876-3804(21)60004-6
- Zhu, X., Zeng, H., Li, S., Dong, Y., Zhu, S., Zhao, D., et al. (2017). Sedimentary Characteristics and Seismic Geomorphologic Responses of a Shallow-Water Delta in the Qingshankou Formation from the Songliao Basin, China. *Mar. Petroleum Geol.* 79, 131–148. doi:10.1016/j.marpetgeo.2016.09.018
- Zou, H., Li, Q.-L., Bagas, L., Wang, X.-C., Chen, A.-Q., and Li, X.-H. (2021). A Neoproterozoic Low- $\delta^{18}O$ Magmatic Ring Around South China: Implications for Configuration and Breakup of Rodinia Supercontinent. *Earth Planet. Sci. Lett.* 575, 117196. doi:10.1016/j.epsl.2021.117196
- Zou, H., Wang, J., Chen, A., Zhong, Y., Chen, H., Liu, S., et al. (2020). Sedimentology of the Deltaic Paleogene Shahejie Formation in the D-1 Area of Liaodong Bay, East China. *Geol. J.* 55 (12), 7738–7759. doi:10.1002/gj.3901

Conflict of Interest: DZ was employed by Xinjiang Oilfield Company.

DZ was employed by Turpan-Hami Oilfield Company.

The remaining authors declare that the research was conducted in the absence of any commercial or financial relationships that could be construed as a potential conflict of interest.

Publisher's Note: All claims expressed in this article are solely those of the authors and do not necessarily represent those of their affiliated organizations, or those of the publisher, the editors, and the reviewers. Any product that may be evaluated in this article, or claim that may be made by its manufacturer, is not guaranteed or endorsed by the publisher.

Copyright © 2022 Zhi, Liu, Chen, Said, Tang, Hu, Qin, Zou and Gong. This is an open-access article distributed under the terms of the Creative Commons Attribution License (CC BY). The use, distribution or reproduction in other forums is permitted, provided the original author(s) and the copyright owner(s) are credited and that the original publication in this journal is cited, in accordance with accepted academic practice. No use, distribution or reproduction is permitted which does not comply with these terms.